An aeroacoustic investigation into the effect of self-oscillating trailing edge flaplets

Edward Talboys [*1], Thomas F. Geyer[2], and Christoph Brücker[1]

[1]*City, University of London, Northampton Square, London, EC1V 0HB, United Kingdom*
[2]*Brandenburg University of Technology Cottbus - Senftenberg, 03046 Cottbus, Germany*

Abstract

The aeroacoustics of a NACA 0012 aerofoil with an array of self-oscillating flexible flaplets attached to the trailing edge has been investigated at low to moderate chord based Reynolds number (50,000 – 350,000) and at geometric angles of attack from $\alpha_g = 0° - 20°$. Two distinct situations were tested: one in which the flaplets were attached to the pressure side, tangentially extending the surface down the trailing edge; the other is with the flaplets attached to the suction side and extending this surface, respectively. For the reference aerofoil, strong tonal peaks are observed. When the passive flaplets are attached to the pressure side, these tonal peaks are removed and the overall sound pressure level (OSPL) is reduced by up to 20 dB. If the flaplets are placed on the suction side, the noise reduction is still present but not as strong as compared to the other case. It is concluded that the case with flaplets on the pressure side is more beneficial in interrupting the feedback loop between the boundary layer instabilities and noise sources in the wake as it is seemingly modifying the laminar separation bubble situated on the pressure side of the aerofoil, the major tonal noise source. The somewhat lower overall noise reduction obtained by the case with flaplets attached on the suction side is suggested to result from the upstream stabilisation in the boundary layer on the suction side by the mechanism of lock-in as show in a recent paper by Talboys and Brücker (2018).

1   Introduction

Aerofoil self-noise reduction is a topic which is attracting increasing interest due to the growing need and desire for 'quieter' aerofoils for various engineering applications. The main source of this self-noise is the boundary layer – trailing edge interaction. Therefore various strategies have been proposed by engineers in recent years to mitigate this.

For moderate Reynolds numbers, when the boundary layer flow along the aerofoil is still in the laminar state, a strong tonal noise is present. As such is especially annoying for the human hearing spectrum, a significant amount of research has been carried out in order to try to understand this phenomenon. The first detailed study of this tonal noise was done by Paterson et al. (1972). Their observations show that the main tonal peak frequency initially scales with the freestream velocity $U_\infty^{0.8}$ until sudden jumps

---

to higher frequencies are observed, which is commonly referred to as 'laddering'. If those 'laddering' events are averaged out over a large frequency range, the scaling changes to $U_\infty^{1.5}$. Tam (1974) built off these results and proposed an aeroacoustic interaction between instabilities in the boundary layer of the aerofoil and noise sources situated in the wake, which self-enforce as a feedback loop. Arbey and Bataille (1983) then expanded on Tam's feedback model by showing that indeed Tollmien-Schlichting (T-S) waves in the boundary layer initiate the feedback when defracting at the trailing edge. There they create acoustic waves, which back-scatter upstream and feed the loop. This conclusion initiated more detailed investigations into the flow field around the aerofoil. Lowson et al. (1994) and McAlpine et al. (1999) showed that the tonal noise is governed by the presence of a laminar separation bubble on the pressure side of the aerofoil and that the frequency of the tonal noise is the most amplified frequency in the boundary layer by using linear stability theory. Desquesnes et al. (2007) carried out the first direct numerical simulation (DNS) on the tonal noise issue and they found that another feedback loop co-exists with the previously described one, which originates from the instabilities on the suction side of the aerofoil. This feedback was then thought to modulate the discrete frequencies which are evenly spaced around the main tonal peak. Pröbsting et al. (2015) later showed that one of the two co-existing feedback mechanisms dominates the overall sound pressure level, of which depends on the Reynolds-number range. This conclusion was achieved by simultaneous measurements of the flow field by Particle Image Velocimetry (PIV) and the acoustic field with microphone-arrays. Their results show that the tonal noise generation at very low chord based Reynolds numbers (Re_c = 30,000) is controlled by the suction side, while at higher Reynolds numbers (Re_c = 230,000) it is dominated by the pressure side. By tripping either side of the aerofoil separately, it is demonstrated that both feedback loops can exist independently (Desquesnes et al., 2007).

Many different techniques have been investigated to mitigate boundary-layer trailing edge noise generation, most of which are inspired from the well-known 'silent' flight of the owl. Geyer et al. (2010) investigated a wide range of aerofoils with different porosities, inspired from the 'soft downy feathers' of the owl. Even a small porosity showed already an aeroacoustic benefit in the low to mid frequency range, of which effect increases with increasing porosity, even in some cases reaching up to 10 dB broadband noise reduction. However, this came with a penalty of noise increase in the high frequency range originating from the modified surface roughness of the aerofoil. In addition, both lift and drag forces were negatively effected compared to the non porous aerofoil.

Another owl-inspired technique uses trailing edge brushes or serrations, mimicking the characteristic trailing edge structure formed by the feathers of owls. Brushes were observed to reduce noise in the high-frequency range 2–16 kHz (Herr, 2007), probably affecting mostly the broadband noise of the turbulent boundary layer interacting with the trailing edge. Finez et al. (2010) could show that the spanwise coherence of the shed vorticies in the wake behind the trailing edge is reduced by 25% in the presence of brushes. Serrations have been extensively researched in both the laminar boundary layer case (Chong et al., 2010) and turbulent boundary layer case (Arce León et al., 2017). Their mechanism in noise reduction is - similar to the brushes - through the reduction of spanwise coherence in the shed vortices. Studies with a single flexible flap at the trailing edge were investigated by Schlanderer and Sandberg (2013). They carried out a DNS study on a flat plate with an elastic compliant trailing edge and found an aeroacoustic benefit at low and medium frequencies with an increased noise level at the Eigen frequency of the material. These results were confirmed later by Das et al. (2015) in an experimental investigation using a similar arrangement to Schlanderer and Sandberg (2013). Active oscillations of a trailing edge flap were studied by Jodin et al. (2018). Their investigation was focused on the wake structure and it was observed that the wake could be reduced in thickness by as much as 10%.

In the present study, a novel configuration of a flexible trailing edge is used, consisting of an array of individual elastic flaplets mimicking the tips of bird feathers aligned along the span of the wing. This type of trailing edge modification with arrays of individual mechanical oscillators in form of elastic flaps has thus far only studied by the authors (Kamps et al. (2016, 2017); Geyer et al. (2019)). Attached to the trailing edge of a NACA 0010 aerofoil, the rows of individual silicone flaplets clearly showed a

(a) Schematic display of the measurement setup (top view, × marks the location of the single microphone)

(b) Photo of the NACA 0012 aerofoil with the flaplets adhered on the trailing edge.

(c) Showing the two different flaplet placements at an angle of incidence, α. Pressure side placement (top) and suction side placement (bottom)
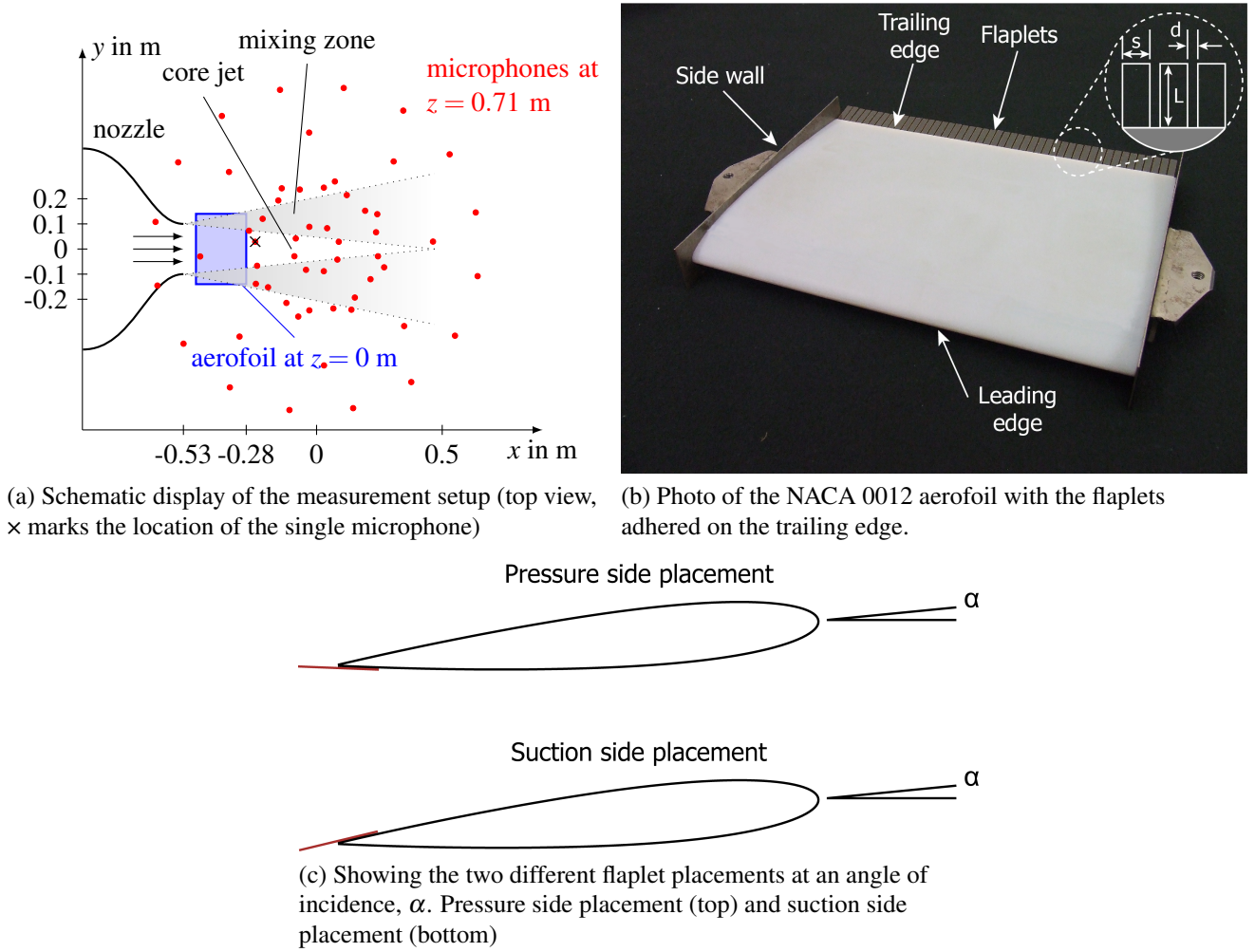
Figure 1: Experimental set-up

reduction in tonal noise (Kamps et al. (2017)). A follow-up study on the flow modification by this type of trailing edge was done by Talboys and Brücker (2018) and demonstrated aerodynamic advantages as well. Detailed High-Speed PIV measurements, coupled with simultaneous motion recordings of the flap tips, prove a stabilisation mechanism of the flaps on the boundary layer on the suction side. A lock-in was triggered by tuning the fundamental frequency of the structural bending mode of the oscillator to match with the fundamental frequency of the shear-layer on the suction side, forming regular vortex rollers in the boundary layer. This lock-in delays the growth of non-linear instabilities such as the merging of the rollers, beneficially affecting also the overall aerodynamic performance. The present study builds on this previous work in order to provide a more in-depth aeroacoustic analysis on the benefits of such self-oscillating flaplets at the trailing edge. In addition, hot wire measurements of the turbulent velocity fluctuations in the wake of the airfoils provide insight into the effect of the flaplets on the flow field.

2   Experimental Arrangement

The aerofoil used for the present study was a NACA 0012, with a chord (c) of 0.2 m and a span (s) of 0.28 m. The model was 3D printed giving the aerofoil a trailing edge bluntness of 0.5 mm with a solid angle of 16°. The flexible trailing edge flaplets were manufactured, using a laser cutter, from a thin polyester film (see table 1 for dimensions and material properties). The flaplets were attached to the aerofoil using a thin strip of double sided tape, and placed such that the free ends were orientated downstream at 1.1c, allowing them to freely oscillate at their Eigen frequency in the flow field. The Eigen frequency was determined to be 107 Hz in a previous study (Talboys and Brücker, 2018), using

Length (L)	Width (s)	Inter spacing (d)	Thickness	Density	Young's Modulus	Eigen frequency
20 mm	5 mm	1 mm	180 μm	1440 kg/m^3	3.12 GPa	107 Hz

Table 1: Flaplet Dimension and Material Properties

cantilever beam theory. The flaplets were placed on both sides of the aerofoil, separately, in order to observe if the there is any effect depending on whether the flaplets were orientated tangentially with the pressure or suction side.

The acoustic and hot wire anemometry (HWA) measurements took place in the small aeroacoustic open jet wind tunnel (Sarradj et al., 2009) at the Brandenburg University of Technology in Cottbus, with a setup similar to that used in Geyer et al. (2010). The wind tunnel was equipped with a circular nozzle with a contraction ratio of 16 and an exit diameter b of 0.2 m. With this nozzle, the maximum flow speed is in the order of 90 m/s and at 50 m/s, the turbulence intensity in front of the nozzle is below 0.1 %. For the present study the chord based Reynolds number was varied from 50,000 – 350,000 and the geometric angle of attack, α_g, was varied from $\alpha_g = 0°$ to 20°. As the wind tunnel is open jet, a correction factor is commonly applied to the angle of attack. This correction factor was introduced by Brooks et al. (1986) who used lifting line theory to account for the deflection induced by the open jet boundary conditions. However due to the small jet width to aerofoil chord ratio ($b/c = 1$), the correction factor should be used with caution (Moreau et al., 2003) and as such has not been used to indicate the angle in the present study. All angles, unless otherwise stated, are therefore the geometric angles of attack (α_g). During measurements, the wind tunnel test section is surrounded by a chamber with absorbing walls on three sides, which lead to a quasi anechoic environment for frequencies above 125 Hz.

For the measurements, the aerofoil was positioned at a distance of 0.05 m downstream of the nozzle. The tips of the aerofoil were attached to a six component wind tunnel balance to simultaneously measure the integral aerodynamic forces. Since the span of the aerofoil ($s = 0.28$ m) exceeded the nozzle diameter, no aerodynamic noise was generated at the tips or the lateral mountings. A schematic of the setup is shown in Fig. 1a.

The acoustic measurements were performed using a planar microphone array, consisting of 56 1/4th inch microphone capsules flush mounted into an aluminium plate with dimensions of 1.5 m × 1.5 m (see Sarradj (2010)). The microphone layout is included in Fig. 1a. The aperture of the array is 1.3 m. The array was positioned out of the flow, in a distance of 0.71 m above the aerofoil.

Data from the 56 microphones were recorded with a sampling frequency of 51.2 kHz and a duration of 60 s using a National Instruments 24 Bit multichannel measurement system. To account for the refraction of sound at the wind tunnel shear layer, a correction method was applied that is based on ray tracing (Sarradj (2017)). In post processing, the time signals were transferred to the frequency domain using a Fast Fourier Transformation (Welch's method, Welch (1967)), which was done blockwise on Hanning-windowed blocks with a size of 16384 samples and 50 % overlap. This lead to a small frequency spacing of only 3.125 Hz. The resulting microphone auto spectra and cross spectra were averaged to yield the cross spectral matrix. This matrix was further processed using the CLEAN-SC deconvolution beamforming algorithm proposed by Sijtsma (2007), which was applied to a two-dimensional focus grid parallel to the array and aligned with the aerofoil. The grid has a streamwise extent of 0.5 m, a spanwise extent of 0.4 m and an increment of 0.005 m. The outcome of the beamforming algorithm is a two-dimensional map of noise source contributions from each grid point, a so-called sound map. In order to obtain spectra of the noise generated by the interaction of the turbulent boundary layer with the trailing edge of the aerofoil, a sector was defined that only contains the noise source of interest. The chosen sector has a chordwise extent of 0.2 m and a spanwise extent of 0.1 m. Thus, spectra of the noise generated by this mechanism are derived by integrating all noise contributions from within this sector, while all potential background noise sources (such as the wind tunnel nozzle or the aerofoil leading edge) are excluded from the integration. The resulting sound pressures were then converted to sound pressure

levels L_p *re* 20 μPa and 6 dB were subtracted to account for the reflection at the rigid microphone array plate. In addition to the beamforming results, auto spectra of a single array microphone close to the aerofoil trailing edge were analysed. The microphone position is highlighted in Fig.1a.

The HWA measurements were taken in separate experiments to the acoustic measurements, to insure no additional noise from the HWA and associated traverse system was measured in the acoustic spectra. The probe used was a Dantec X wire probe (55P64), where the data was taken at a sampling frequency of 25.6 kHz. The Dantec HWA hardware system used for the measurements contains an electronic low-pass filter with a cut-off frequency of 10 kHz. The wake profiles were initiated at $0.25c$ above the aerofoil till $0.25c$ below the aerofoil, at a distance of $0.25c$ from the solid aerofoil edge approximately at mid span. The increment of the measurements was large in the freestream region (1 mm), and then the increment was systematically reduced such that the region of the boundary layer was measured with 0.2 mm increments. Each measurement was taken for a period of 10 sec, prior to moving on to the next increment. Longer measurements were taken, directly behind the trailing edge such that the spectra of the turbulent velocity fluctuations of the wake could be analysed. The measurement period for these measurements was 60 sec. These measurements were converted to the frequency domain using Welch's method, which was done on rectangular windowed blocks of 65536 samples with an overlap of 50 %, leading to a frequency spacing of 0.39 Hz.

3   Results

3.1   Theoretical Comparison

Brooks, Pope and Marcolini (BPM) (Brooks et al., 1989) created a semi-empirical model that aims to predict the aerofoil self-generated noise by breaking it down into five main components; laminar boundary layer – trailing edge interaction (LBL–TE), turbulent boundary layer – trailing edge interaction (TBL–TE, both on suction and pressure sides), separated flow noise, trailing edge bluntness and tip vortex noise. As the aerofoil used in the present study is bounded by two end plates, the tip vortex noise is not considered. In order to use this model to predict and analyse the noise sources the open source software, NAFNoise (Moriarty, 2005), was used. NAFNoise uses a panel method, Xfoil, to calculate the necessary boundary layer parameters for the model and has an additional feature which uses a simplified version of the Guidati model, to calculate the additional noise induced from a turbulent inlet flow. As mention in Section 2, the inflow turbulence is low for the present experimental set-up; nonetheless this has still been accounted for in the prediction.

Figure 2 shows the comparison of the BPM model with the reference experimental results at $\alpha_g = 0°$, for all of the Reynolds numbers tested. The contours have been normalised by their respective maximum SPL in order to compare the overall trends. Immediately it can be seen that in Fig. 2a, there is a clear trend of increasing tonal peak with Reynolds number. This trend corresponds well with the empirical $Re_c^{1.5}$ scaling from Paterson et al. (1972). As the results from the BPM model are in third octave bands, the 'laddering' effect, which scales as $Re_c^{0.8}$, cannot be seen and only the average effect is observed. In the experimental results, Fig. 2b, the trend is also clearly visible and hence the BPM model can be used for the current experimental set-up over a wide range of Reynolds numbers to help to understand the noise sources.

Fig. 3 shows the BPM prediction against the experimental results for the baseline case and both of the flaplet orientation cases for one Reynolds number, 300,000 and at two different geometric angles of attack. In general the BPM model can predict the frequency of the tonal peak at both angles of attack well, however the magnitude is over predicted. The LBL-TE noise is the dominating source in both cases, which is to be expected as transition is not forced. In the $0°$ case (Fig. 3a), it can be seen that in the higher frequency range the pressure/suction side TBL (only the pressure side TBL has been plotted in Fig. 3a) becomes the dominating noise source, but the influence on the overall noise level is small in relation to the LBL-TE tonal peak. As the angle increases, Fig. 3b, the predicted tonal peak also increases
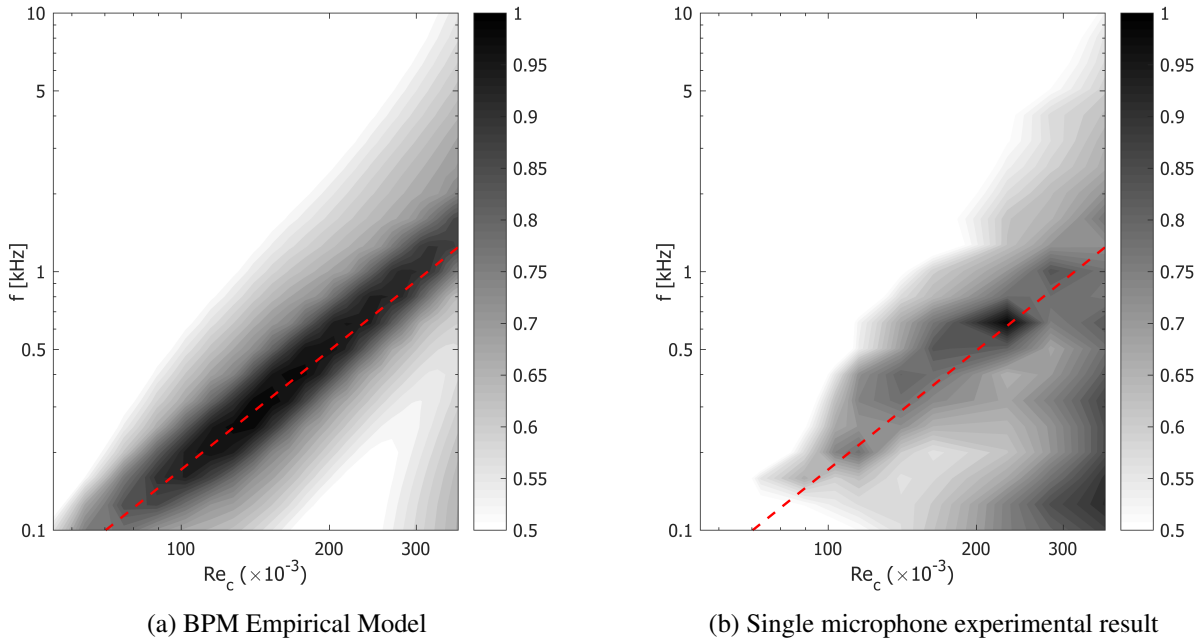
(a) BPM Empirical Model

(b) Single microphone experimental result

Figure 2: Contours of normalised third octave band SPL across the Reynolds number range studied at $\alpha_g = 0°$. The contours are normalised by their respective maximum SPL. The --- shows the $\sim Re_c^{1.5}$ trend line observed by Paterson et al. (1972)
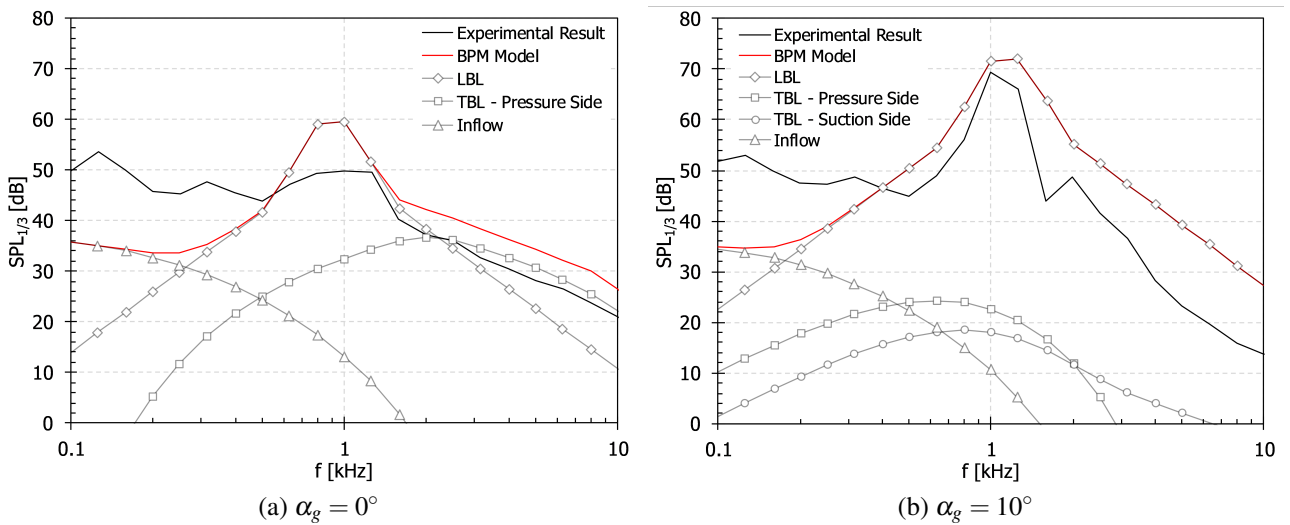

(a) $\alpha_g = 0°$

(b) $\alpha_g = 10°$

Figure 3: Comparison of the third octave sound pressure level (SPL$_{1/3}$) at Re_c = 300,000 between experimental result and the BPM prediction model. Where the BPM model is the summation of the laminar boundary layer (LBL) noise, both the pressure and suction side turbulent boundary layer (TBL) noise and the turbulent inflow noise.

in amplitude and the turbulent noise sources no longer affect the predicted spectra.

3.2   Single Microphone Measurements

Fig. 4 shows the single microphone measurements from the microphone situated vertically above the trailing edge, see Fig. 1a. For clarity, each Reynolds number test is spaced with an increment of 30 dB from the previous test case, their corresponding Reynolds number is labeled next to each group of spectra. At zero incidence, Fig. 4a, it can be seen that for all Reynolds numbers a tonal peak can be observed. An interesting observation can be seen in the low frequency range (0.1 kHz – 0.4 kHz) where there is a
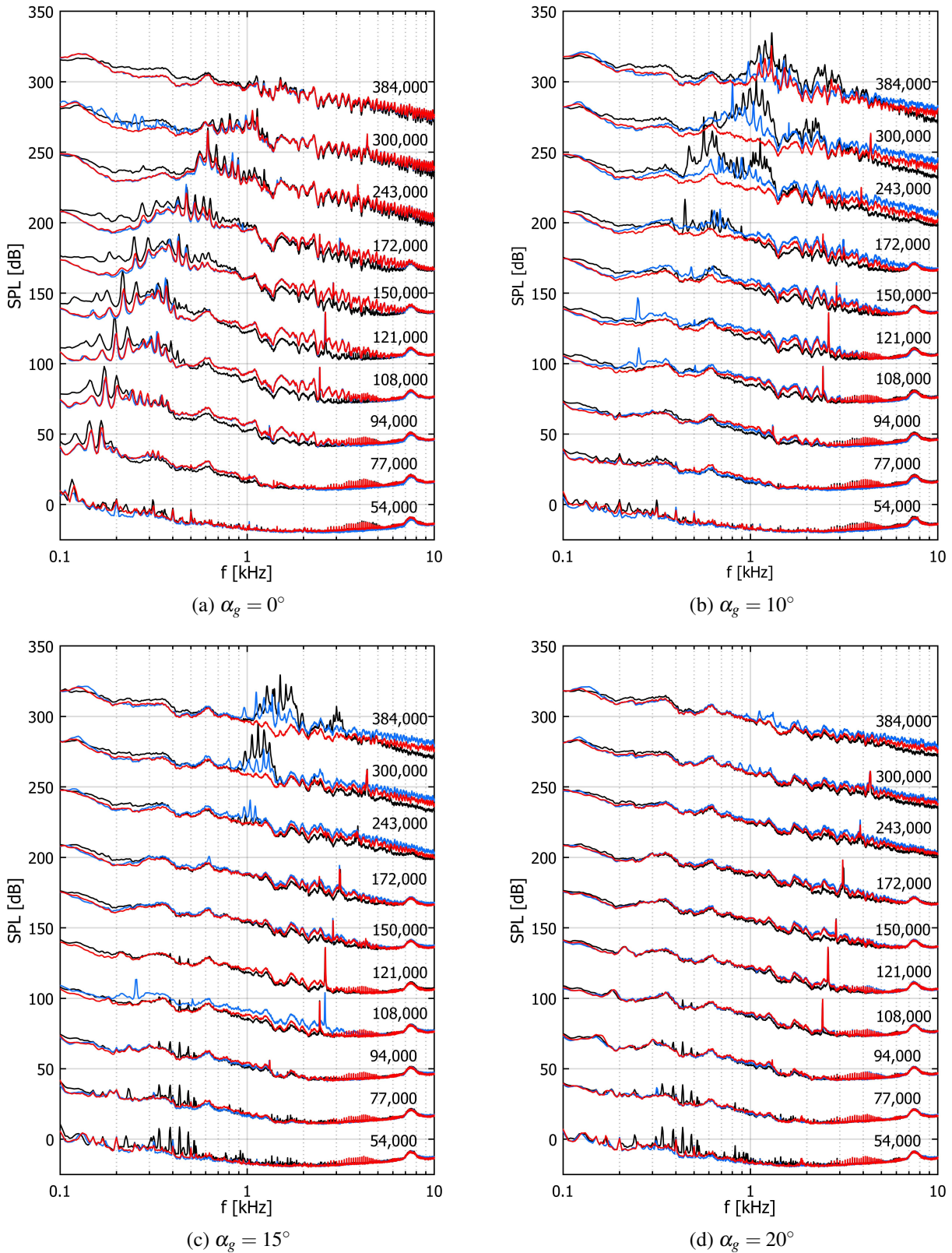
Figure 4: Single microphone measurements for each Reynolds number case, are spaced with 30dB increments for clarity. Each of the angles stated are the geometric angles of attack. For each angle and Reynolds number there are three test cases: a baseline case with no flaplets (—), the case where the flaplets are affixed to the pressure side (—) and when the flaplets are affixed onto the suction side (—).

significant reduction in the noise level across all cases once the flaplets are applied. There is no preference in the surface placement of the flaplets. However, this is expected due to the symmetry of the aerofoil at

$\alpha_g = 0°$. The reduction that is seen is thought to be related to the vortex shedding noise which is changed due to the flaplets modifying the wake. This reduction of vortex shedding noise has been observed on a cylinder with flexible elements on the aft half of the cylinder (Kamps et al., 2016; Geyer et al., 2019). Jodin et al. (2017) have showed that by using a similar, but active, trailing edge modification the wake structure is modified and it is this type of flow modification that is thought to be the mechanism behind the low frequency noise reduction. It can be seen that the reduction in the low frequency range has been scattered into the medium to high frequency range (~ 1 kHz). As the Reynolds number is increased, the reduction in the low frequency and the high frequency increase both reduce. This is postulated to be due to the low Eigen frequency of the current flaplet geometry, and therefore these benefits observed are limited to a finite low frequency range.
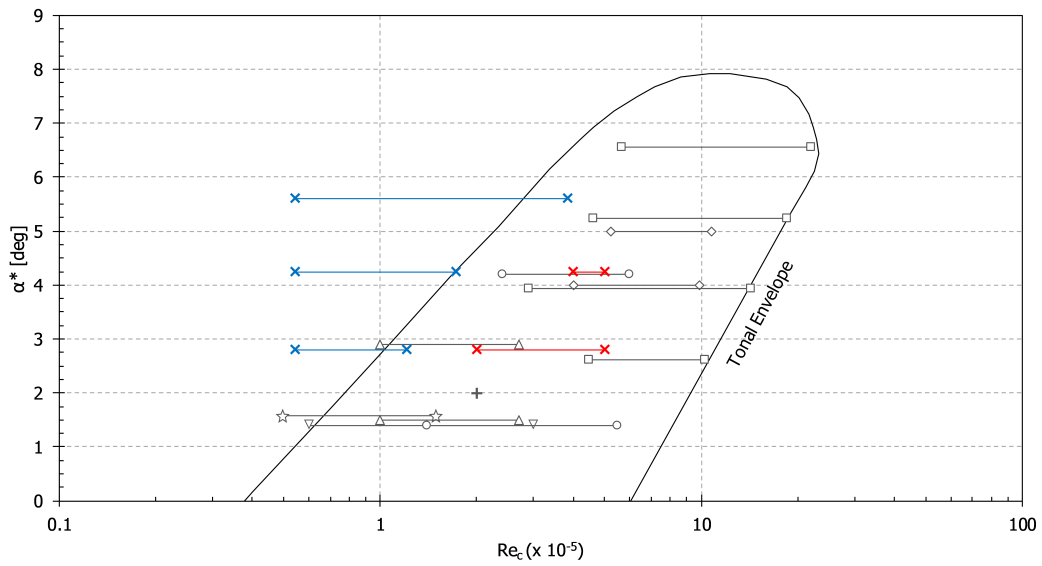

Figure 5: Comparison of previous literatures and the present study in the tonal noise envelope for the NACA 0012 aerofoil as proposed by Lowson et al. (1994). The angle of attack (α^*) is corrected using the BPM empirical correction for the open jet wind tunnel results. Neither the direct numerical simulation (DNS) or closed wind tunnel angles have been adjusted. □ Paterson et al. (1972); ◇ Lowson et al. (1994); + Desquesnes et al. (2007); ▽ Inasawa et al. (2013); ○ Chong et al. (2013); △ Pröbsting et al. (2014); ☆ Arcondoulis et al. (2018); ✕ Present (tonal) and ✕ Present (non-tonal)

As the angle increases to $\alpha_g = 10°$, Fig. 4b, a tonal peak starts to emerge at 450 Hz for the reference case at $Re_c = 172,000$. As the Reynolds number increases further the tonal peaks in the baseline case increase in frequency and intensity. The tonal peaks which are observed for this angle of attack and the subsequent angles agree well with the 'tonal envelope' model, Fig.5, which was first proposed by Lowson et al. (1994), when the angle is normalised using the empirical scaling factor (Brooks et al., 1986). A series of previous publications using the NACA 0012 have also been normalised, accounting for different experimental set-ups, and fall within this tonal envelope.

A particularly interesting result can be first seen in Fig. 4b, where the placement of the flaplets on the pressure side of the aerofoil significantly reduces or removes the tonal frequencies. Whereas the placement on the suction side does not have such a profound impact. However, it should be noted that the peaks are slightly reduced. The low frequency reduction is also observed, but is reduced compared to that of the zero incidence case. This suppression of tonal noise is also seen at $\alpha_g = 15°$, Fig. 4c, at the higher Reynolds number cases. At $\alpha_g = 20°$, Fig. 4d, there is no real discernible difference between the two flaplet orientations due to the test cases being outside the tonal envelope. The low frequency noise reduction can still be seen at higher incidences, however it is reduced and has a trend of reducing as Reynolds number and α_g increase, in a similar fashion to that of the $\alpha_g = 0°$ case.

3.3   Linear stability analysis

As detailed by Lowson et al. (1994) and McAlpine et al. (1999), the most amplified instability wave in the boundary layer, prior to the separation bubble on the pressure side, is very close to that of the tonal frequency observed. They also stated that a separation bubble on the pressure side is a necessary requirement in the production of tonal noise on the NACA 0012 aerofoil. Therefore a linear stability analysis (LSA) has been carried out on the $\alpha_g = 10°$ cases where the tonal peaks were observed (i.e. the top three cases in Fig. 4b). The LSA was carried out using the Airbus Callisto boundary-layer solver (a more detailed overview of the methods used in the solver can be found in Atkin (2014) and the references therein). In summary, Callisto has three distinct stages; obtaining the pressure distribution of an aerofoil (using the Callisto Viscous Garabedian and Korn method), produce boundary profiles for each station on the aerofoil and then carry out a stability analysis. In the present study the pressure distributions are created using Xfoil, which are then imported in to the QinetiQ BL2D solver. Due to the limitations of the open jet correction factor, the true angle of attack is unknown. Therefore, the measured lift forces were used in order to iterate the pressure distribution, such that the correct pressure distribution can be found. BL2D then uses a standard finite-difference, parabolic solver which is based on Horton and Stock (1995) to produce boundary layer profiles up to the transition point. These profiles are subsequently then analysed using QinetiQ CoDS, which is the linear stability analysis solver. CoDS uses an e^N method to obtain the N-Factors of the boundary layer profiles, and as such it can produce an amplification curve for each boundary layer profile. In the present results, Fig. 6, the non-dimensional spatial growth rate, $-\alpha_i \delta^*$, is plotted against modal frequency (f), where δ^* is the local displacement thickness of the boundary layer and α_i is the imaginary part of the spatial growth rate. A negative α_i indicates an unstable mode, hence the maxima in the $-\alpha_i \delta^*$ curves show the most unstable mode and the corresponding frequency it occurs at. As the current aerofoil was modelled as a semi-infinite 2D model, only Tollmien-Schlichting (T-S) waves are responsible for the instability growth.

(a) $Re_c = 243,000$; $\alpha_g = 10°$ (b) $Re_c = 300,000$; $\alpha_g = 10°$ (c) $Re_c = 384,000$; $\alpha_g = 10°$
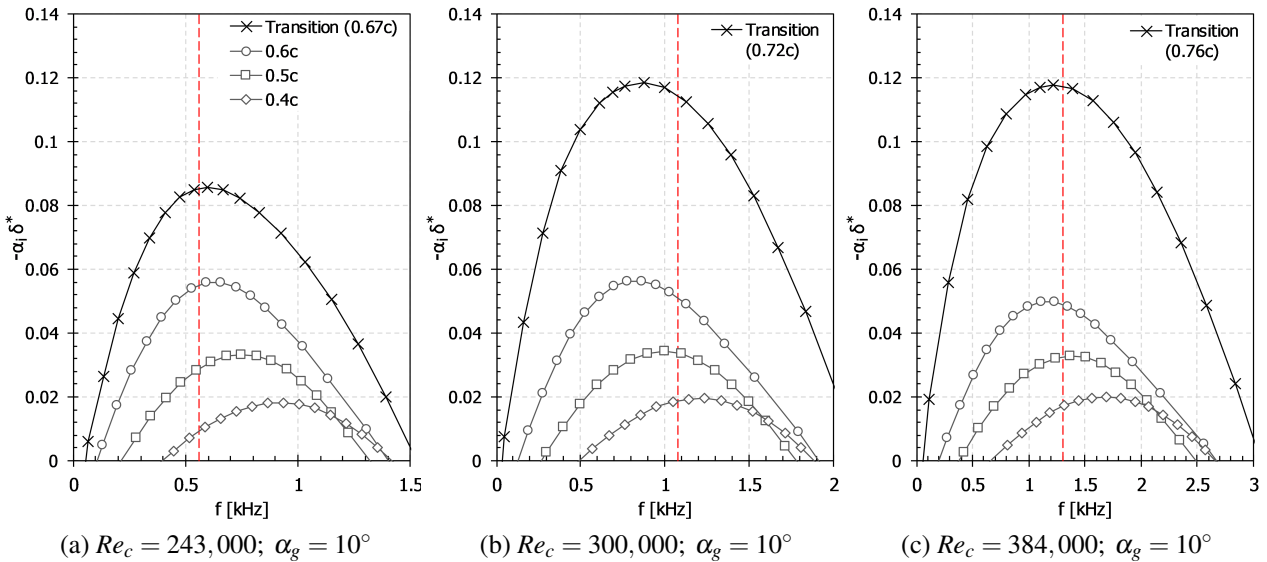
Figure 6: The spatial growth rate on the pressure side of the aerofoil at different chordwise positions (x/c) against the frequency at which they occur. (- - -) Indicates the frequency where the tonal peak (f_n) is observed in the experiment, see Fig. 4b.

The general trend, that can be seen in Fig. 6, is that the spatial growth rate of the instabilities increases in amplitude as they are convected downstream. The most amplified modal frequency also becomes more defined. Eventually non-linear effects take over, shortly followed by a breakdown to turbulence. As such the linear stability analysis is not valid beyond this point. The most amplified frequency in the boundary layer can therefore be found at the point prior to when these non-linear instabilities take over forming

a laminar separation bubble (LSB). When comparing the frequency at which this maximum growth rate occurs, to the corresponding experimental tonal peaks (see Fig. 4b), good agreement between both sets can be seen. The addition of the flaplets on the pressure side of the aerofoil creates a small step (measured to be 0.28 mm) at a chordwise position of 0.85c, which is in the region of this separation bubble. This could trigger transition earlier and as such the LSB is not present. Therefore the tonal noise component is removed, as the presence of a LSB is a prerequisite for tonal noise (Lowson et al., 1994).

3.4 Overall sound pressure level measurements

Fig. 7 shows the overall sound pressure level (OSPL) obtained by beamforming as described in Section 2. The OSPL is a means of summing all of the acoustic contributions from each frequency in the signal to give one numerical value for each test case (see Eqn. (1)). In order to easily quantify the effects numerically, the difference between the corresponding baseline and flaplet cases (see Eqn. 2) has been analysed as well.

$$\text{OSPL} \quad = \quad 10\log_{10}\left[\sum_i 10^{\text{SPL}_i/(10\text{ dB})}\right] \tag{1}$$

$$\Delta\text{OSPL} \quad = \quad \text{OSPL}_{\text{flaplet}} - \text{OSPL}_{\text{baseline}} \tag{2}$$

(a) $\alpha_g = 0°$

(b) $\alpha_g = 10°$
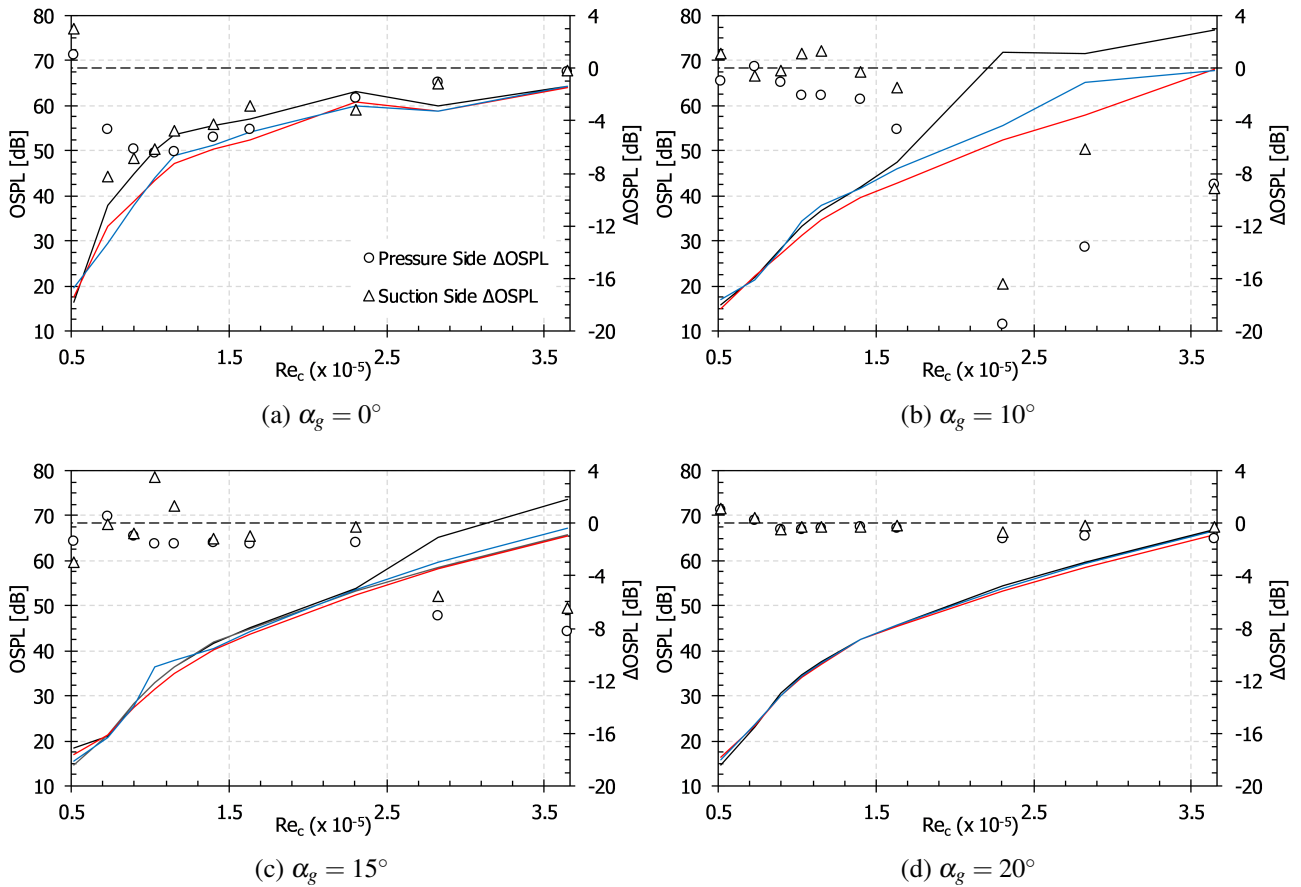
(c) $\alpha_g = 15°$

(d) $\alpha_g = 20°$

Figure 7: Overall sound pressure levels for the reference cases and the flaplet, pressure side mounted, cases. ΔOSPL has been plotted on the second axis to yield a clear indication of the difference at each Reynolds number. The zero line on the ΔOSPL axis is shown as (---). Reference (—), flaplets pressure side mounted (—) and flaplets suction side mounted (—). ○ Indicates the ΔOSPL of the pressure side mounted flaplets and △ indicates the ΔOSPL of the suction side mounted flaplets.

For the $\alpha_g = 0°$ case, Fig. 7a, it can be seen that both flaplet orientations lead to a reduction of ~5-7 dB up to a Reynolds number of 250,000. Then beyond this, the overall noise reduction approaches zero. The large reduction in the low Reynolds number range is due to the observed low frequency reduction in Fig. 4a. Then at the higher velocities the smaller low frequency reduction cancels out with the high frequency noise increase. For the increased angles, where tonal noise is observed (Fig. 7b and 7c), the trend is the opposite. The low Reynolds number cases show little or no noise reduction. But as Reynolds number increases, the tonal noise component starts to emerge on the reference aerofoil and as such the reduction becomes much more profound. At $\alpha_g = 10°$, noise reductions of up to ~16-20 dB can be seen and ~6-8 dB can be seen at $\alpha_g = 15°$. As was seen in Fig. 4b and 4c, the suction side flaplets do not show as much noise reduction as the pressure side flaplets. This is due to a reduced tonal noise suppression and an increased noise level at high frequencies. At $\alpha_g = 20°$, there are very little differences between all the cases, resulting in minimal noise reduction benefits. Table 2 gives the averaged ΔOSPL for each of the angles.

α_g	0°		10°		15°		20°	
Pressure/suction side flaplet placement	P	S	P	S	P	S	P	S
Average ΔOSPL [dB]	-3.62	-3.47	-5.49	-3.07	-2.48	-1.35	-0.41	-0.09

Table 2: Average ΔOSPL for each of the geometric angles of attack (α_g). A placement of 'P' indicates that the flaplets are affixed to the pressure side and 'S' indicates a suction side placement.

3.5   Aerodynamic force measurements

The integral aerodynamic forces were taken simultaneously with the acoustic measurements for the current study. Due to the open jet flow conditions, the exact span that is subjected to the flow is not precisely known. Therefore the lift and drag forces have been normalised by their respective baseline measurement, to give an indication of relative performance difference.

$$F_L^* = \frac{F_{L,i}}{F_{L,ref(i)}} \tag{3}$$

$$F_D^* = \frac{F_{D,i}}{F_{D,ref(i)}}, \tag{4}$$

In Eqns. (3) and (4), $F_{L,i}$ and $F_{D,i}$ are the measured lift and drag for the cases with the flaplets, while $F_{L,ref(i)}$ and $F_{D,ref(i)}$ are the corresponding forces of the reference aerofoil at the same Reynolds number and geometric angle of attack. Therefore a value of $F_L^* > 1$ means an increase in lift compared to the baseline and vice versa for a values less than 1. The same reasoning holds for F_D^*. A generic trend can be seen in Fig. 8, where the pressure side placement decreases drag and lift and the suction side placement increases both lift and drag. At $\alpha_g = 20°$, the trend does not hold where the pressure side cases have an increased drag, but with comparable lift. This trend is in agreement with a basic XFLR simulation, where the flaplet orientation (as indicated in Fig. 1c) alters the circulation of the aerofoil and hence the aerofoil performance. As the Reynolds number increases, it is also seen in both cases, that the results converge to the centre of the polar. The results for $\alpha_g = 0°$ have been omitted due to very small values observed for the lift, due to the symmetry of the aerofoil, and as such any deviation gives a very large F_L^*.

3.6   Hot wire anemometry

The mean flow profile and fluctuation statistics in the wake of the aerofoils were measured with a hot-wire traversed in y-direction at a distance of $0.25c$ downstream of the solid trailing edge. The measurements
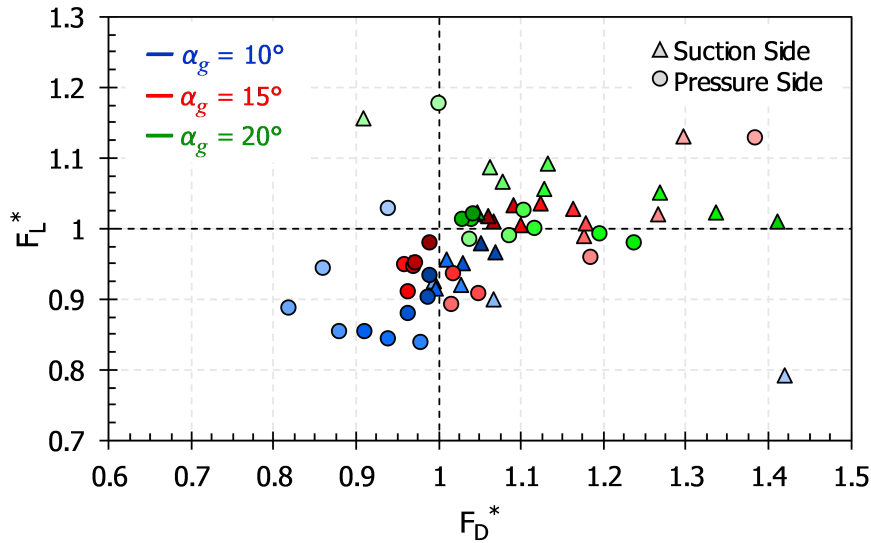
Figure 8: Normalised lift and drag measurements for all cases, where the shading of the colours indicates the Reynolds number. A lighter shade indicates a lower Reynolds number and the darker shade indicates the higher Reynolds number cases.

with the attached flaps were all compared to the reference case at the same position and angle of incidence. The mean profiles in Fig. 9a demonstrate an increased wake deficit for both flaplet cases compared to the plain aerofoil. Partly, this effect is due to the extension of the chord by the presence of the attached flaps, which in effect extend the trailing edge to 1.1c. Therefore, in the cases with attached flaps the boundary layer will grow further and the resulting wake deficit at the measurement location should be larger. When comparing only the two different cases with flaplets, it is seen that the deficit, in the case of the flaplets attached to the pressure side, is not as pronounced as in the suction side case. In addition, it has also a somewhat smaller width of the wake, which indicates a lower drag. This is in agreement with the observations seen in Fig. 8.

The effect of the flaplets is more evident when comparing the statistics of the velocity fluctuations, u_{RMS}, as shown in the profiles in Fig. 9b. The reference case exhibits overall significantly higher values than both of the flaplet cases, with a pronounced lobe on the pressure side of the aerofoil. The rms-profiles for the cases with attached flaplets show two distinct lobes, with the broader of the two situated on the suction side of the aerofoil, associated with the thicker shear layer on this side. The larger peak of both lobes in each rms-profile is always found on the same side, where the flaplets were attached.

The turbulence spectra of the streamwise velocity fluctuations (u') are displayed in Fig. 10, normalised by a nominal value of $\Phi_0 = 1$ m^2/s. For clarity, the suction side and pressure side spectra have been spaced with -10 dB increments from the reference case to distinguish between the plots presented in the same figure. The reference case clearly illustrates the strong tonal peak at about 700 Hz, together with the first harmonic at 1.4 kHz. In addition, a pair of fringe frequencies, equispaced by 70 Hz on either side of the spectral peak is visible, similar as those observed by Pröbsting et al. (2014). When the flaplets are attached to the aerofoil, one can clearly see the beneficial modification of the spectrum along the tonal peak. When attached to the pressure side, the flaps lead to a complete disappearance of the frequency peaks corresponding to the tonal noise. In comparison, when the flaps were attached to the suction side a tonal peak is still visible at a similar peak frequency range as for the plain aerofoil, however at lower energy ($\sim$ 13 dB lower) as the first harmonic is not present. In addition, there is no indication of any fringe frequencies. The results furthermore demonstrate the beneficial effect of the flaps at the trailing edge, similar as it was observed earlier in the flow studies reported by Talboys and Brücker (2018). In conclusion, the flaps lead to a redistribution of energy from velocity fluctuations in certain frequency bands towards a more broadband spectrum. The positive feedback of the lock-in of the oscillating flaps onto the fundamental instability of the boundary layer on the suction side has already
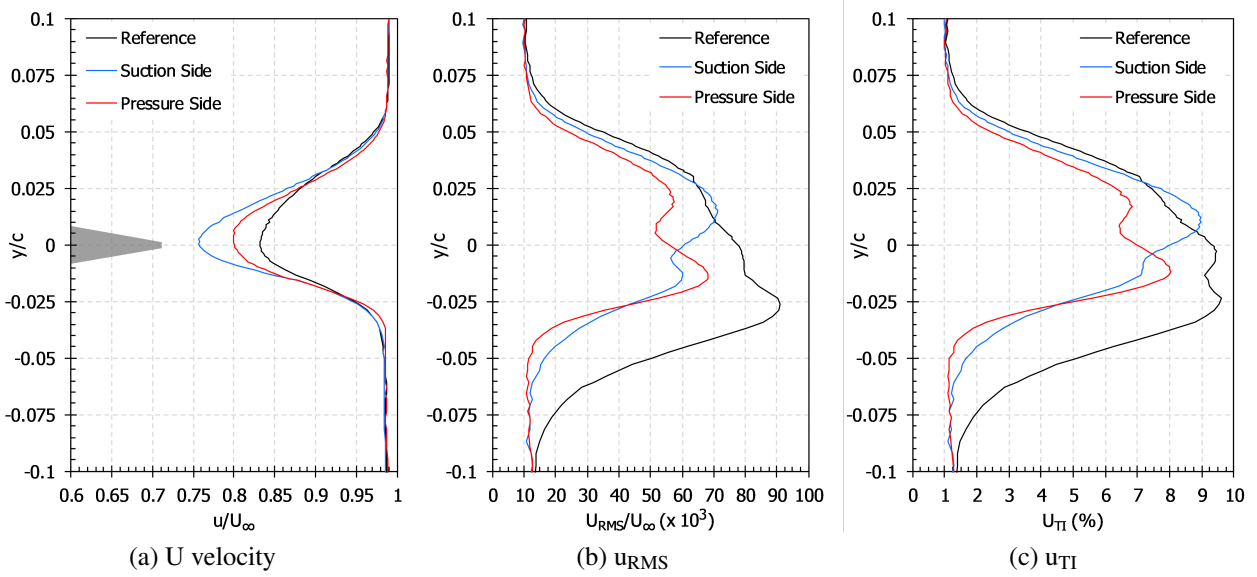
(a) U velocity   (b) u_{RMS} (c) u_{TI}

Figure 9: Hot wire anemometer results of the streamwise component (u) for the case at $Re_c = 243,000$ and $\alpha_g = 10°$. The shaded area in Fig. 9a is a graphical representation of the reference aerofoil orientation with respect to the profile measurements.

been proven by detailed flow measurements (Talboys and Brücker (2018)). Therefore we suggest that the observed cancellation of the fringe frequencies is related to this lock-in effect. Pröbsting et al. (2014) argued that the fringe frequencies are caused by the modification of vortical structures convecting over the surface, which are affected by a back-scatter effect when those structures shed from the trailing edge. We found these vortical structures to be rollers in the shear-layer as a consequence of the fundamental instability. The flaps had clearly an influence on delaying the non-linear interaction of these rollers. This could indicate that the presence of the oscillating flaplets damps the related pressure fluctuations associated with these interactions. This hypothesis is somewhat supported by the u_{RMS} values and the turbulence intensities shown in Fig. 9b and 9c, respectively, where a large reduction in both is observed on the pressure side of the aerofoil.
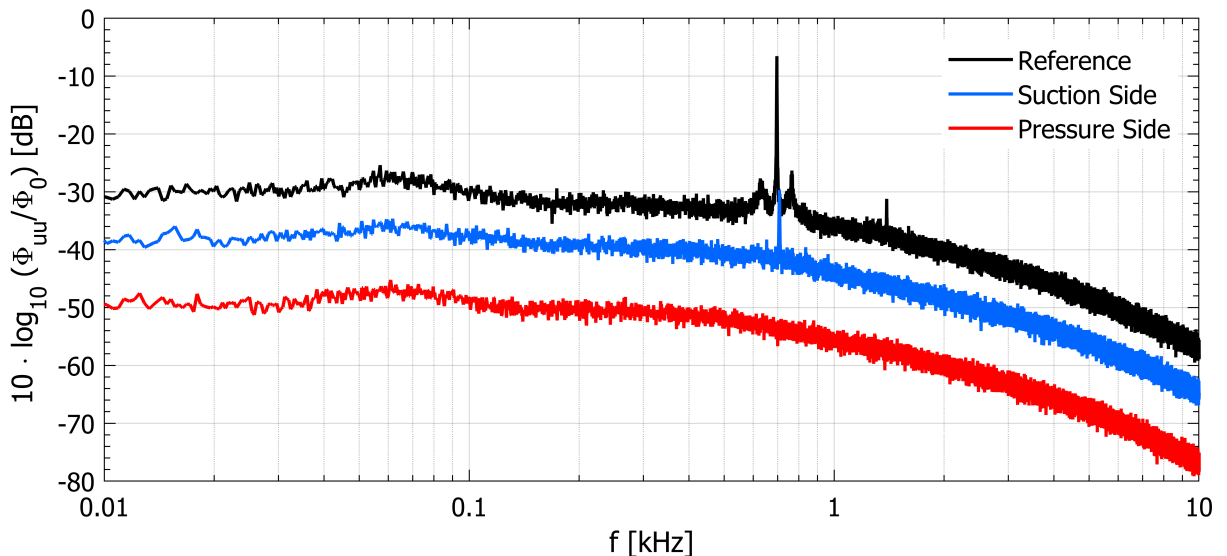

Figure 10: Fluctuating streamwise velocity turbulence spectra (Φ_{uu}), normalised with $\Phi_0 = 1 \text{ m}^2/\text{s}$, behind the trailing edge for the untripped case at $Re_c = 243,000$ and $\alpha_g = 10°$

4   Conclusion

Aeroacoustic measurements with a microphone-array were carried out in an anechoic chamber for the flow along a NACA0012 aerofoil in order to observe the acoustic effect of a trailing edge with attached flexible passive flaplets (bending beam oscillators). The measurements focus on moderate Reynolds number flows in the range 50,000 – 350,000 at geometric angles of attack $\alpha_g = 0° - 20°$, where strong tonal peaks are observed on the baseline case consistent with previous literature Desquesnes et al. (2007). Two distinct situations were tested: one in which the flaplets were attached to the pressure side, tangentially extending the surface down the trailing edge; the other is with the flaplets attached to the suction side and extending this surface, respectively. Both configurations have a clear beneficial effect on reducing the tonal noise. For the case with the flaplets attached to the pressure side the tonal peaks even are completely cancelled out and the overall sound pressure level (OSPL) is reduced by up to 20 dB. This is suggested to be due to a modification to the laminar separation bubble on the pressure side, which is the key mechanism for tonal noise. High-Speed PIV measurements are currently under way in our lab to further elucidate the dynamics of the separation bubble. On the suction side, the flaplets are known from Talboys and Brücker (2018) to stabilise the shear-layer rollers developing in the boundary layer via a lock-in mechanism. As a result of this self-sustained fluid-structure interaction, pressure fluctuations on the surface linked to any non-linear interaction of the rollers are expected to be reduced by attaching those flexible elements. Indeed, also for this case is a reduction in low frequency noise observed. This results in an overall noise reduction of $\sim 1.5 - 2$ dB over the whole range of Reynolds numbers. The findings from the acoustic measurements are complemented with results from aerodynamic force measurements as well as hot wire anemometry measurements in the wake. For the case with flaplets on the suction side, the force measurements show also a benefit in aerodynamic performance by increasing the lift. This results is consistent with recent flow simulations for a NACA0012 with an actively controlled trailing edge undergoing harmonic oscillations (Jodin et al., 2017). Note, that the described aeroacoustic observations are only valid for the specific flap geometry and mechanical properties chosen, consistent with the previous flow study reported in Talboys and Brücker (2018). For a more global conclusion, the studies should incorporate the effect of different flaplet length, width and inter-spacing. This is currently being investigated in our lab.

Acknowledgements

References

Arbey H, Bataille J (1983) Noise generated by airfoil profiles placed in a uniform laminar flow. J Fluid Mech 134(-1):33, DOI 10.1017/S0022112083003201

Arce León C, Merino-Martínez R, Ragni D, Avallone F, Scarano F, Pröbsting S, Snellen M, Simons DG, Madsen J (2017) Effect of trailing edge serration-flow misalignment on airfoil noise emissions. J Sound Vib 405:19–33, DOI 10.1016/j.jsv.2017.05.035

Arcondoulis E, Zander A, Doolan CJ, Brooks L, Liu Y (2018) Airfoil dual acoustic feedback mechanisms at low-to-moderate Reynolds number. In: 2018 AIAA/CEAS Aeroacoustics Conf., American Institute of Aeronautics and Astronautics, Reston, Virginia, DOI 10.2514/6.2018-3936

Atkin C (2014) Convergence of calculated transition loci during computational analysis of transonic aerofoils and infinite swept wings. In: 29th Congr. Int. Counc. Aeronaut. Sci., St. Petersburg, Russia

Brooks TF, Marcolini MA, Pope DS (1986) Airfoil trailing-edge flow measurements. AIAA J 24(8):1245–1251, DOI 10.2514/3.9426

Brooks TF, Pope S, Marcolini MA (1989) Airfoil Self-Noise and Prediction. NASA Ref Publ 1218 pp 1–142, DOI 10.1080/09524622.2008.9753825

Chong TP, Joseph P, Gruber M (2010) An Experimental Study of Airfoil Instability Noise with Trailing Edge Serrations. In: 16th AIAA/CEAS Aeroacoustics Conf., American Institute of Aeronautics and Astronautics, Reston, Virigina, vol 332, pp 6335–6358, DOI 10.2514/6.2010-3723

Chong TP, Joseph PF, Kingan MJ (2013) An investigation of airfoil tonal noise at different Reynolds numbers and angles of attack. Appl Acoust 74(1):38–48, DOI 10.1016/j.apacoust.2012.05.016

Das C, Mimani A, Porteous R, Doolan C (2015) An experimental investigation of flow-induced noise mechanism of a flexible flat-plate trailing-edge. Annu Conf Aust Acoust Soc 5(1):1–10

Desquesnes G, Terracol M, Sagaut P (2007) Numerical investigation of the tone noise mechanism over laminar airfoils. J Fluid Mech 591:155–182, DOI 10.1017/S0022112007007896

Finez A, Jondeau E, Roger M, Jacob MC (2010) Broadband noise reduction with trailing edge brushes. Proc 16th AIAA/CEAS aeroacoustics Conf pp 1–13

Geyer TF, Sarradj E, Fritzsche C (2010) Measurement of the noise generation at the trailing edge of porous airfoils. Exp Fluids 48(2):291–308, DOI 10.1007/s00348-009-0739-x

Geyer TF, Kamps L, Sarradj E, Brücker C (2019) Vortex Shedding and Modal Behavior of a Circular Cylinder Equipped with Flexible Flaps. Acta Acust united with Acust 105(1):210–219, DOI 10.3813/AAA.919301

Herr M (2007) Design Criteria for Low-Noise Trailing-Edges. 13th AIAA/CEAS Aeroacoustics Conf (28th AIAA Aeroacoustics Conf pp 1–14, DOI 10.2514/6.2007-3470

Horton HP, Stock HW (1995) Computation of compressible, laminar boundary layers on swept, tapered wings. J Aircr 32(6):1402–1405, DOI 10.2514/3.46893

Inasawa A, Ninomiya C, Asai M (2013) Suppression of Tonal Trailing-Edge Noise From an Airfoil Using a Plasma Actuator. AIAA J 51(7):1695–1702, DOI 10.2514/1.J052203

Jodin G, Motta V, Scheller J, Duhayon E, Döll C, Rouchon JF, Braza M (2017) Dynamics of a hybrid morphing wing with active open loop vibrating trailing edge by time-resolved PIV and force measures. J Fluids Struct 74:263–290, DOI 10.1016/j.jfluidstructs.2017.06.015

Jodin G, Rouchon JF, Scheller J, Triantafyllou M (2018) Electroactive morphing vibrating trailing edge of a cambered wing : PIV , turbulence manipulation and velocity effects. In: IUTAM Symp. Crit. flow Dyn. Involv. moving/deformable Struct. with Des. Appl., Santorini, Greece

Kamps L, Geyer TF, Sarradj E, Brücker C (2016) Vortex shedding noise of a cylinder with hairy flaps. J Sound Vib 388:69–84, DOI 10.1016/j.jsv.2016.10.039

Kamps L, Brücker C, Geyer TF, Sarradj E (2017) Airfoil Self Noise Reduction at Low Reynolds Numbers Using a Passive Flexible Trailing Edge. In: 23rd AIAA/CEAS Aeroacoustics Conf., American Institute of Aeronautics and Astronautics, Reston, Virginia, June, pp 1–10, DOI 10.2514/6.2017-3496

Lowson M, Fiddes S, Nash E (1994) Laminar boundary layer aero-acoustic instabilities. In: 32nd Aerosp. Sci. Meet. Exhib., American Institute of Aeronautics and Astronautics, Reston, Virigina, DOI 10.2514/6.1994-358

McAlpine A, Nash E, Lowson M (1999) On the Generation of Discrete Frequency Tones by the Flow around an Aerofoil. J Sound Vib 222(5):753–779, DOI 10.1006/jsvi.1998.2085

Moreau S, Henner M, Iaccarino G, Wang M, Roger M (2003) Analysis of Flow Conditions in Freejet Experiments for Studying Airfoil Self-Noise. AIAA J 41(10):1895–1905, DOI 10.2514/2.1905

Moriarty P (2005) NAFNoise User ' s Guide

Paterson RW, Vogt PG, Finkt MR, Munch CL (1972) Vortex Noise of Isolated Airfoils. NACA Adv Restricted Rept 3G29 J Aeronaut Sci J Aircr Low Adv Ration J Am Helicopter Soci-ety J Aircr 17(5):3–12, DOI 10.2514/3.60229

Pröbsting S, Serpieri J, Scarano F (2014) Experimental investigation of aerofoil tonal noise generation. J Fluid Mech 747(2):656–687, DOI 10.1017/jfm.2014.156

Pröbsting S, Scarano F, Morris SC (2015) Regimes of tonal noise on an airfoil at moderate Reynolds number. J Fluid Mech 780:407–438, DOI 10.1017/jfm.2015.475

Sarradj E (2010) A fast signal subspace approach for the determination of absolute levels from phased microphone array measurements. J Sound Vib 329(9):1553–1569, DOI 10.1016/j.jsv.2009.11.009

Sarradj E (2017) A fast ray casting method for sound refraction at shear layers. Int J Aeroacoustics 16(1-2):65–77, DOI 10.1177/1475472X16680463

Sarradj E, Fritzsche C, Geyer TF, Giesler J (2009) Acoustic and aerodynamic design and characterization of a small-scale aeroacoustic wind tunnel. Appl Acoust 70(8):1073–1080, DOI 10.1016/j.apacoust.2009.02.009

Schlanderer SC, Sandberg RD (2013) DNS of a Compliant Trailing-Edge Flow. In: 19th AIAA/CEAS Aeroacoustics Conf., American Institute of Aeronautics and Astronautics, Reston, Virginia, pp 1–18, DOI 10.2514/6.2013-2013

Sijtsma P (2007) CLEAN Based on Spatial Source Coherence. Int J Aeroacoustics 6(4):357–374, DOI 10.1260/147547207783359459

Talboys E, Brücker C (2018) Upstream shear-layer stabilisation via self-oscillating trailing edge flaplets. Exp Fluids 59(10):145, DOI 10.1007/s00348-018-2598-9

Talboys E, Geyer TF, Brücker C (2018) The Aerodynamic And Aeroacoustic Effect Of Passive High Frequency Oscillating Trailing Edge Flaplets. In: IUTAM Symp. Crit. flow Dyn. Involv. moving/deformable Struct. with Des. Appl., Santorini, Greece

Tam CKW (1974) Discrete tones of isolated airfoils. J Acoust Soc Am 55(6):1173–1177, DOI 10.1121/1.1914682

Welch P (1967) The use of fast Fourier transform for the estimation of power spectra: A method based on time averaging over short, modified periodograms. IEEE Trans Audio Electroacoust 15(2):70–73, DOI 10.1109/TAU.1967.1161901